Society of Exploration Geophysicists, 72nd Annual International Meeting, 2002
Expanded Abstracts, 2393-2396.
LAUR 02-2033

A comparison of microseismicity induced by gel-proppant- and water-injected hydraulic fractures, Carthage Cotton Valley gas field, East Texas

J.T. Rutledge and W.S. Phillips, Los Alamos National Laboratory*

Summary

We have improved the location precision and computed focal mechanism of microearthquakes induced during a series of hydraulic fracture completions within the Cotton Valley formation of East Texas. Conventional gel-proppant treatments and treatments using treated water and very low proppant concentrations (waterfracs) were monitored. Waterfracs have been shown to be just as effective as the conventional gel-proppant treatments in Cotton Valley reservoirs, but at greatly reduced cost (Mayerhofer and Meehan, 1998). Comparison of the seismicity induced by the two treatment types show similar distributions of event locations and focal mechanisms for common depth intervals. We interpret the induced seismicity to be primarily controlled by the natural fracture geometry and independent of treatment design. By implication, we expect the effectiveness of shear-induced fracture propping to be independent of the treatment fluid in Cotton Valley reservoirs.

Introduction

In May and July, 1997, a consortia of operators and service companies conducted a series of hydraulic fracture imaging tests in the Carthage Cotton Valley gas field of East Texas (Walker, 1997). Microseismic data were collected and processed for six hydraulic fracture treatments in two wells (3 completion intervals per well) (Mayerhofer et al., 2000). One well was completed with gel-proppant treatments in which a viscous crosslink gel was injected to entrain high concentrations of sand proppant into formation. The second well was completed using treated water and very low proppant concentrations (waterfracs). Waterfracs have been shown to be just as effective as the conventional gel-proppant treatments in Cotton Valley reservoirs, but at greatly reduced cost. Mayerhofer and Meehan (1998) suggest two possible reasons why waterfracs are successful: 1) Induced shear displacement along natural and hydraulic fractures results in self-propping (shear dilation enhanced by fracture branching, proppant and spalled rock fragments), and 2) Fracture extension and cleanup is easier to achieve with low-viscosity fluids. With improved source location precision and focal mechanism determination (fracture plane orientation and sense of slip), we have re-examined the Cotton Valley data, comparing the seismicity induced by water and gel-proppant treatments at common depth intervals.

Operational set up

The treatment and monitor wells are shown in Figure 1. Two 2350-ft-long, 48-level, 3-component geophone arrays were attached to the outside of 2-7/8-inch production tubing and cemented into the monitor wells 22-09 and 21-09. We refer to the 21-09 array as Array-1, and the 22-09 array as Array-2. Geophone stations were spaced at 50 ft intervals. Signals were amplified 60 dB downhole, with an additional 48 dB of gain applied uphole before digitizing the waveforms at a 1-ms sample interval. Details on the instrumentation design and installation are presented in Walker (1997). For this study we used data from subsets of geophone stations that spanned the completion zones and the entire operating lengths of the arrays (Rutledge and Phillips, 2002).

Well 21-10 was completed with gel-proppant treatments and was monitored using both arrays. Afterwards well 21-09 was completed by waterfrac and monitored using Array-2 only. The treatment data for both wells are summarized in Mayerhofer et al. (2000). Because well 21-09 was completed with small-diameter casing, injection rates were limited to 8 to 10 barrels per minute (bpm), whereas the 21-10 gel-proppant treatments were pumped at 40 bpm. The restricted injection rates in 21-09 also required smaller depth intervals to be treated separately. Total injected fluid volumes in 21-09 were also reduced to about two-thirds of the 21-10 treatments, over their common depth intervals. The common treatment intervals presented here are within the Upper Cotton Valley formation, a thick (~800 ft) sequence of interbedded sands, siltstones and shales (for details see Walker, 1997). Well casings are perforated over 10- to 20-ft intervals targeting specific productive sand intervals.

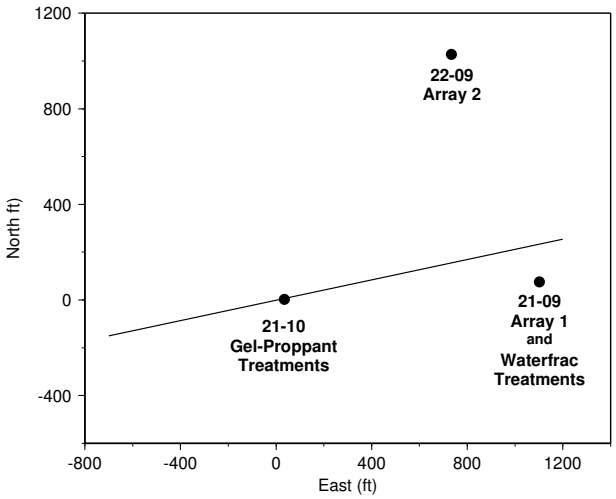

Figure 1. Treatment and monitor wells. The line through the treatment well is the anticipated hydraulic fracture orientation based on stress measurements (Laubach and Monson, 1988).

Source re-location and focal mechanism analysis

We re-located the microearthquake sources after obtaining precise arrival-time data by systematic and consistent repicking of events with similar waveforms (e.g., Phillips, 2000). Events that occur repeatedly on the same fault plane or along adjacent, similarly-oriented fault planes produce nearly identical waveforms at a receiver station if they result from the same sense of slip. We repicked the events in spatial sequence along the treatment lengths. The similarity of waveforms observed in

this process allowed us to visually correlate waveforms (Rutledge and Phillips, 2002). We also upsampled the data from a 1-ms to a 0.2-ms sample interval using a finite-impulse-response (FIR) interpolation filter (Vaidyanathan, 1990). Subsample arrival-time precision was obtained from the interpolated data by consistently picking easily identified peaks or troughs within the first half cycle of P- and S-phases. On average, we reduced the standard deviation of arrival-time misfits 4-fold from the original pick data (observed minus predicted arrival times), resulting in a 4-fold reduction in relative location error (Rutledge and Phillips, 2002).

Applying precise location techniques also aids in determining focal mechanisms of the induced events that are otherwise difficult to solve with sparse receiver networks. Planar structures resolved by precise locations, for example, can provide independent slip-plane orientations to constrain the focal mechanism. The source coverage can also be expanded by solving for an assumed, common mechanism of the similar-waveform event groups (composite focal mechanisms). We have solved composite focal mechanisms for the Cotton Valley data with groupings based on waveform similarity and discrete location clusters. We use Snoke et al.'s (1984) focal-mechanism routine with a combination of P and SH polarities and the amplitude ratios of SH/P, SV/P and SV/SH as input to constrain the solutions. In some cases the event groups are spatially extensive enough to uniquely constrain solutions with P polarities alone.

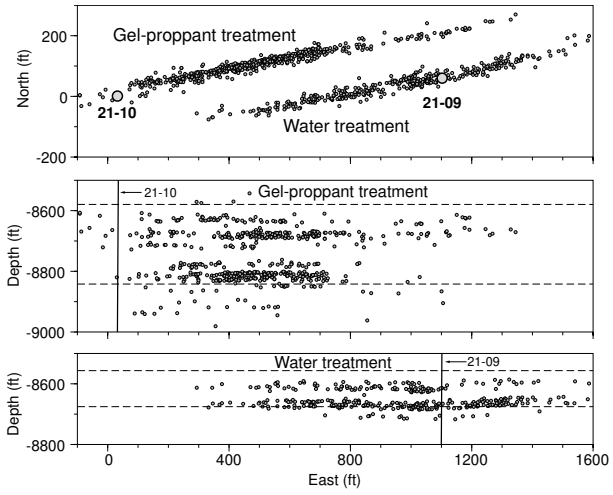

Figure 2. The gel-proppant and waterfrac treatments in wells 21-10 and 21-09, respectively. The dashed lines in the depth views mark the treatment intervals. Six discrete perforation intervals, targeting a total of 80 ft of sand, were simultaneously treated in well 21-10 over a 265-ft interval. The 21-09 treatment covers the upper half of the 21-10 treatment, with 3 discrete perforation intervals totaling 40 ft of targeted sands over a 120-ft interval.

Results

Top of the Upper Cotton Valley. Microseismic locations for the shallowest completion intervals of the Upper Cotton Valley are displayed in Figure 2. Only the eastern wing of the 21-10 treatment is displayed. Both the gel-proppant and waterfrac treatments resulted in 30- to 40-ft wide zones of induced events. Treatment lengths for the waterfrac are about two-thirds of the length attained by the gel-proppant treatment; Mayerhofer et al., (2000) attribute this to the restricted injection rates and smaller fluid volumes pumped in 21-09. The event trends are parallel at N80°E, consistent with independent measurements of maximum horizontal stress (σ_{Hmax}) direction (Laubach and Monson, 1988). The depth views show nearly identical banding and distribution of event locations over their common depth intervals (Figure 2). The banding correlates with the discrete perforation intervals (targeted sands) and the proppant radioactive (RA) tracer logs run in the treatment wells (Rutledge and Phillips, 2001).

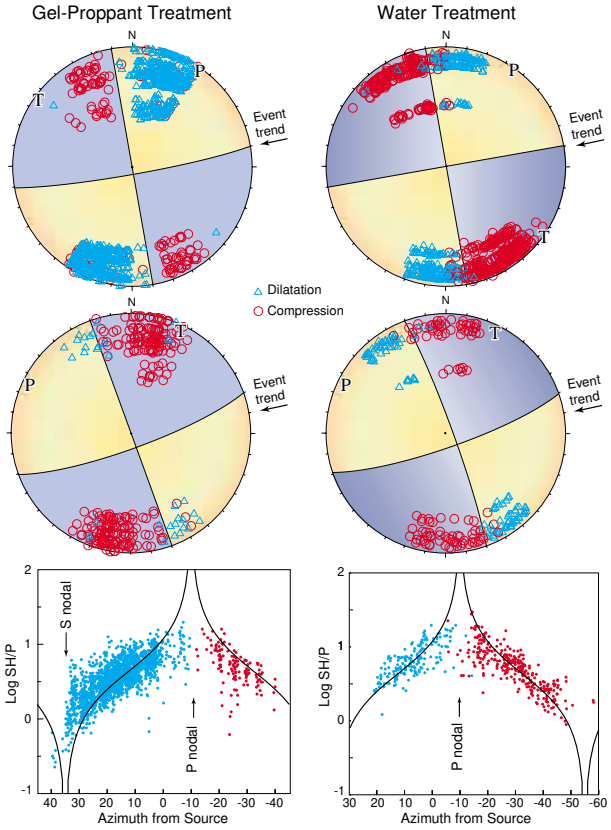

Figure 3. Composite focal mechanism fitting the gel-proppant- and waterfrac-induced events of Figure 2. SH/P amplitude ratios are also shown as a function of the azimuth from event to Array-2. The SH/P values are from the more populous event sets fitting the left-lateral strike-slip solutions. The curves are the theoretical SH/P amplitude ratios for the focal mechanism solutions at top (vertical strike-slip fault striking N80°E).

Repicking the waveforms in sequences along the treatment lengths revealed a gradual waveform evolution and a flip in P-polarities corresponding to a peak in SH/P amplitude ratio. For both treatments the sense of P-polarity change is correlated with SH polarity (Rutledge and Phillips, 2002). From this relationship, we formed two groups based on SH polarities and computed composite focal mechanisms constrained by the P-wave polarity data alone. The majority of events for both treatments had left SH first motions (90% and 82% for the gel-proppant and waterfrac treatments, respectively). The remaining events had right SH first motions (at source, looking

at receiver Array-2). All the focal-mechanism groups uniquely converged to strike-slip solutions consistent with their SH motions and with only 4 to 5% discrepant P-wave first motions (Figure 3). SH/P amplitude ratios are also consistent with the first-motion-constrained, strike-slip solutions (Figure 3). Both treatments resulted in two similar focal mechanisms occurring uniformly over the entire treatment lengths.

Base of the Upper Cotton Valley. Event locations and focal mechanisms for the base of the Upper Cotton Valley are displayed in Figures 4, 5 and 6. Similar to the shallower zones, the seismicity is banded corresponding to isolated sand intervals (Figures 4 and 6). Event magnitudes induced at these depths were larger than the shallower completions of Figure 2 (Urbancic and Rutledge, 2000). The large magnitude events occur within tight clusters that strike off angle from the overall treatment trends of N80°E. For the gel-proppant treatment, clusters 1 to 4 account for 65% of the events detected (Figure 4) and cluster 4 alone makes up 42%. Similarly, for the waterfrac, 80% of the events occur within the eastern-most cluster (#5, Figure 6). Focal mechanisms for all but one of these energetic clusters show strike-slip faulting, with the P-axes azimuths close to σ_{Hmax} (N80°E). The other events locations, shown in red, are generally weaker, but occur more extensively and continuous along the treatment lengths (Figures 4 and 6). Most of the red events fit strike-slip focal mechanisms similar to the top of the Cotton Valley (Figure 3), with one nodal plane subparallel to the event-trend and σ_{Hmax} directions (Figure 5 and cluster-2 mechanism of Figure 6).

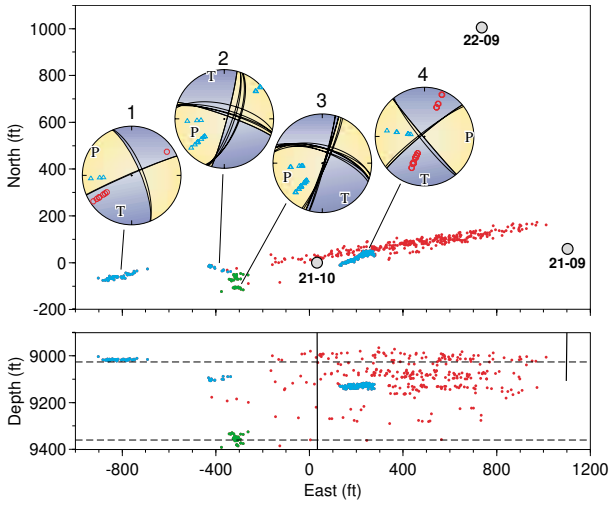

Figure 4. Event locations for the gel-proppant treatment within the base of the Upper Cotton Valley. Four distinct subclusters are shown in blue and green with their respective focal mechanism solutions. Multiple nodal planes show the range of possible solutions.

Interpretation

In Rutledge and Phillips (2001) we presented an interpretation of the locations and focal mechanisms of the uppermost 21-10, gel-proppant treatment (Figures 2 and 3). We briefly summarize that interpretation here since the waterfrac at the same depth shows an identical response.

The prevalent natural fracture orientation within the Cotton Valley is vertical and striking within 10° of σ_{Hmax} (Dutton et al., 1991). We interpret the focal mechanism groups of Figure 3 to represent slip induced on these pre-existing fractures, with the sense of slip determined by the fracture plane's strike relative to σ_{Hmax} direction (~N80°E, parallel to the seismic trends of Figure 2). Both the left- and right-lateral fault-plane solutions show a nodal plane within 10° of the seismic trends, with their respective nodal planes showing the correct sense of rotation with respect to σ_{Hmax} required to flip from left-lateral to right-lateral slip. This relative sense of strike is independently supported by the SH/P data (Rutledge and Phillips, 2001; 2002). The natural fractures are also isolated within individual sands with few, if any, occurring in the intervening shales (Dutton et al., 1991). The bands of seismicity, thereby, are also consistent with activating the pre-existing fracture system.

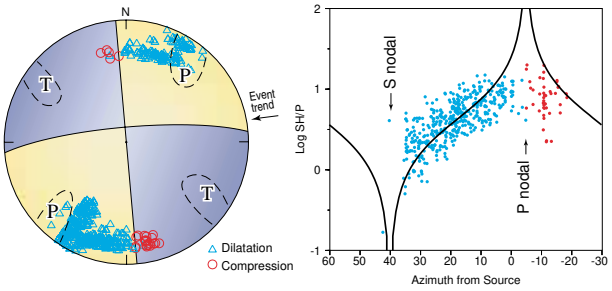

Figure 5. Composite focal mechanism and SH/P amplitude ratios for 64% of events shown in red of Figure 4. Grouping was based on SH and P polarities. 16% of the events shown in red of Figure 4 fit a similarly-oriented right-lateral solution; 20% fit neither.

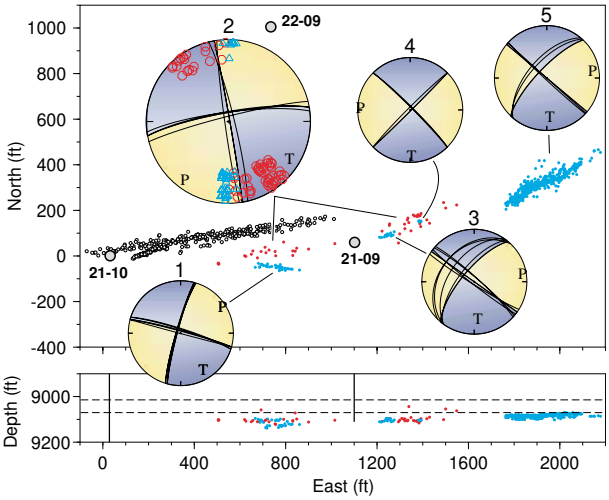

Figure 6. Event locations for the 21-09 waterfrac treatment in the base of the Upper Cotton Valley (red and blue symbols). Event locations are also shown in map view for the eastern wing of the 21-10 gel-proppant treatment (open symbols). The 21-09 treated interval is marked by dashed lines. The seismicity suggests most of the injectate went out the well bottom (21-09) to a permeable horizon below. This depth zone corresponds to one of the most active zones stimulated in 21-10 (Figure 4). The blue clusters (1, 3-5) are the more energetic events; these events have strike-slip focal mechanisms with failure planes off trend of σ_{Hmax}. Most of the events shown in red fit the larger focal mechanism (#2) showing strike slip along fractures trending subparallel to σ_{Hmax}.

Seismicity induced within the deeper Upper Cotton Valley indicates a more heterogeneous population of natural fractures are being pressurized. The event counts and energies are dominated by activation of fractures optimally oriented for strike-slip failure (P- and T-axis trends are close to σ_{Hmax} and σ_{hmin} directions, respectively), but not necessarily optimally oriented for drainage. Cluster 4, for example, is the most populous structure activated during the 21-10 gel-proppant stimulation (Figure 4), but it appears to form a short, dead-end path that developed by events migrating westward (Phillips et al., 2002) from the main trend of seismicity (red events of Figure 4). We presume that the gaps of seismicity in Figures 4 and 6 are filled in with weaker events that are out of detection range or are being missed by the high activity levels on the pressurized fractures with higher resolved shear stresses.

Conclusions

Seismicity induced by conventional gel-proppant and waterfrac treatments in the Upper Cotton Valley formation show similar distributions of event locations and focal mechanisms for common depth intervals.

Within the top of the Upper Cotton Valley, strike-slip shear displacement is induced uniformly along the treatment lengths indicating a pressurized system of vertical fractures trending subparallel to σ_{Hmax}. The focal mechanisms and event locations are consistent with activation of the reservoir's prevalent natural fractures, fractures that are isolated within individual sands and trend subparallel to the expected hydraulic fracture orientation (σ_{Hmax} direction).

Treatments within the base of the Upper Cotton Valley indicate a more heterogeneous fracture system is pressurized. The seismic event counts and energies are dominated by events occurring on fractures with orientations that should have higher resolved shear stress. However, the other, generally weaker events are more extensively and evenly distributed over the treatment lengths, and show the uniform strike-slip mechanisms occurring along near-vertical fractures subparallel to σ_{Hmax}, as in the top half of the Upper Cotton Valley.

These weaker shear events should be associated with more conductive flow paths and higher critical pore pressures. By Coulomb failure criteria, the pore pressure required to induce slip along fractures subparallel to σ_{Hmax} will be relatively high, approaching crack-opening pressures. Hence, incremental pressure increases are likely to extend the shear-active fractures as hydraulic fractures. High pore pressure also implies low effective-normal-stress conditions for slip, a condition that will favor more effective permeability creation via shear dilation (see Evans et al., 1999 and references therein).

We interpret the induced seismicity to be primarily controlled by the natural fracture geometry. Contrary to previous interpretations presented in Mayerhofer et al. (2000) and Urbancic and Rutledge (2000), we find the character of deformation to be independent of treatment design and position from the treatment well. By implication, we expect the effectiveness of shear-induced fracture propping to be independent of the treatment fluid.

Acknowledgment

This work was funded by the Gas Technology Institute and the U.S. Department of Energy's National Petroleum Technology Office. Many thanks to Andi Kron for help with illustrations.

References

Dutton, S.P., Laubach, S.E., Tye, R.S., Diggs, T.N., 1991, Geological analysis of the Travis Peak formation and Cotton Valley sandstone: in Staged Field Experiment No. 3: Application of advanced technologies in tight gas sandstones - Travis Peak and Cotton Valley Formation, Waskom Field, Harrison County, Texas Reservoirs, (Eds.) CER Corp. and S.A. Holditch Assoc., Inc., Gas Research Instit., Report No. GRI-91/0048.

Evans, K.F., Cornet, F.H., Hashida, T., Hayashi, K., Ito, T., Matsuki, K., and Wallroth, T., 1999, Stress and rock mechanics issues of relevance to HDR/HWR engineered geothermal systems: Review of developments during the past 15 years: Geothermics, 28, 455-474.

Laubach, S.E., and Monson, E.R., 1988, Coring-induced fractures: Indicators of hydraulic fracture propagation in a naturally fractured reservoir: Paper 18164, Proc. 1988 Soc. Petro. Eng. Ann. Tech. Conf., Houston, Texas.

Mayerhofer, M.J., and Meehan, D.N., 1998, Waterfracs - Results from 50 Cotton Valley Wells: Paper 49104, Proc. 1998 Soc. Petro. Eng., Ann. Tech. Conf., New Orleans, Louisiana.

Mayerhofer, M.J., Walker, Jr., R.N., Urbancic, T., and Rutledge, J.T., 2000, East Texas Hydraulic Fracture Imaging Project: Measuring hydraulic fracture growth of conventional sandfracs and waterfracs: Paper 63034, Proc. 2000 Soc. Petro. Eng. Ann. Tech. Conf., Dallas, Texas.

Phillips, W.S., 2000, Precise microearthquake locations and fluid flow in the geothermal reservoir at Soultz-sous-Forêts, France: Bull. Seism. Soc. Am., 90, 212-228.

Phillips, W.S., Rutledge, J.T., House, L.S., and Fehler, M.C., 2002, Induced microearthquake patterns in hydrocarbon and geothermal reservoirs, Pure and Applied Geophysics 159, 345-369, 2001.

Rutledge, J.T., and Phillips, W.S., 2002, Natural fracture activation during hydraulic stimulation as revealed by induced microearthquakes, Carthage Cotton Valley gas field, East Texas, Geophysics, in review.

Rutledge, J.T., and Phillips, W.S., 2001, W.S., High-resolution microseismic imaging of a Cotton Valley hydraulic fracture, 71st Ann. Mtg., Soc. of Explor. Geophys., Expanded Abstracts, 404-407.

Snoke, J.A., Munsey, J.W., Eague, A.G., and Bollinger, G.A., 1984, A program for focal mechanism determination by combined use of polarity and SV-P amplitude ratio data, Earthquake Notes, 55, p. 15.

Urbancic, T.I., and Rutledge, J., 2000, Using microseismicity to map Cotton Valley hydraulic fractures: 70th Ann. Mtg., Soc. of Explor. Geophys., Expanded Abstracts, 1444-1448.

Vaidyanathan, P.P., 1990, Multirate digital filters, filter banks, polyphase networks, and applications: A tutorial: Proc. I.E.E.E., 78, 56-93.

Walker, Jr., R.N., 1997, Cotton Valley Hydraulic Fracture Imaging Project: Paper 38577, Proc. 1997 Soc. Petro. Eng. Ann. Tech. Conf., San Antonio, Texas.